CI

e-med
www.e-med.org.uk

ORIGINAL ARTICLE

Texture analysis of non-small cell lung cancer on unenhanced computed tomography: initial evidence for a relationship with tumour glucose metabolism and stage

Balaji Ganeshan[a,b], Sandra Abaleke[a], Rupert C.D. Young[b], Christopher R. Chatwin[b] and Kenneth A. Miles[a]

[a]*Clinical Imaging Sciences Centre, Brighton and Sussex Medical School, Brighton BN1 9RR, UK;* [b]*School of Engineering & Design, University of Sussex, Brighton BN1 9QT, UK*

Corresponding address: Dr Balaji Ganeshan, Clinical Imaging Sciences Centre, Brighton and Sussex Medical School, Brighton, BN1 9RR, UK. Email: b.ganeshan@sussex.ac.uk

Abstract

The aim was to undertake an initial study of the relationship between texture features in computed tomography (CT) images of non-small cell lung cancer (NSCLC) and tumour glucose metabolism and stage. This retrospective pilot study comprised 17 patients with 18 pathologically confirmed NSCLC. Non-contrast-enhanced CT images of the primary pulmonary lesions underwent texture analysis in 2 stages as follows: (a) image filtration using Laplacian of Gaussian filter to differentially highlight fine to coarse textures, followed by (b) texture quantification using mean grey intensity (MGI), entropy (E) and uniformity (U) parameters. Texture parameters were compared with tumour fluorodeoxyglucose (FDG) uptake (standardised uptake value (SUV)) and stage as determined by the clinical report of the CT and FDG-positron emission tomography imaging. Tumour SUVs ranged between 2.8 and 10.4. The number of NSCLC with tumour stages I, II, III and IV were 4, 4, 4 and 6, respectively. Coarse texture features correlated with tumour SUV (E: $r = 0.51$, $p = 0.03$; U: $r = -0.52$, $p = 0.03$), whereas fine texture features correlated with tumour stage (MGI: $r_s = 0.71$, $p = 0.001$; E: $r_s = 0.55$, $p = 0.02$; U: $r_s = -0.49$, $p = 0.04$). Fine texture predicted tumour stage with a kappa of 0.7, demonstrating 100% sensitivity and 87.5% specificity for detecting tumours above stage II ($p = 0.0001$). This study provides initial evidence for a relationship between texture features in NSCLC on non-contrast-enhanced CT and tumour metabolism and stage. Texture analysis warrants further investigation as a potential method for obtaining prognostic information for patients with NSCLC undergoing CT.

Keywords: *Non-small cell lung carcinoma; computed tomography; computer-assisted; lung texture analysis; imaging marker.*

Introduction

Lung cancer is the most common cause of death related to cancer worldwide[1], accounting for more than 1.2 million deaths annually[2]. Non-small cell lung carcinoma (NSCLC) is the most common form of lung cancer prevalent in 80% of all cases[3]. Computed tomography (CT) is widely used for the initial diagnosis and staging of patients with NSCLC and computer-based image analysis has been proposed as a means to improve the diagnostic performance of CT in lung cancer through

improved lesion detection and classification of lesions as benign or malignant[4–10]. There has been interest in using these image analysis methods as part of CT-based lung cancer screening programs and commercial analysis systems are now available[5,11,12].

Although these diagnostic uses of image analysis are well recognised, the application of similar analysis techniques to identify adverse features of lung tumours following diagnosis is largely unexplored. Intratumoural necrosis, haemorrhage and myxoid change are known to cause areas of low attenuation in CT images of lung

and other tumours[13,14]. It is feasible that tumours containing such areas of low attenuation could be recognised by texture analysis methods that quantify local variations in image brightness within a pulmonary lesion. These pathological features are also acknowledged to be associated with increased tumour aggression and it is therefore possible that texture analysis could identify lung tumours with adverse biological characteristics[13,15]. Such information might potentially contribute to the process of tumour staging through additional risk stratification of individual patients. This study aims to undertake a preliminary evaluation of the relationship between CT of NSCLC and tumour glucose metabolism and stage, which are both recognised prognostic factors in lung cancer[16,17].

Materials and methods

This study was performed on archival patient image data that had been acquired as part of an imaging research program to evaluate tumour angiogenesis with a diagnostic contrast-enhanced (CE) CT examination and glucose metabolism using fluorodeoxyglucose (FDG)-positron emission tomography (PET) examination. The Institutional Review Board had approved this research study along with further retrospective image analysis of the data and written consent had been obtained from all patients for the imaging studies.

Patients

This archival retrospective imaging study comprised 17 consecutive patients (11 men and 6 women; mean age 64 years; age range 56–72 years; mean weight 71.5 kg; weight range 45–89 kg), who were recruited by their referring physician, underwent CE CT and FDG-PET as part of their clinical investigation for a lung lesion. FDG-PET and CT were performed within 48 h. Histological examination of biopsy material confirmed 18 NSCLC in 17 patients. Patients were grouped as stage I, II, III or IV using conventional CT criteria for tumour size and local invasion and PET assessments of nodal and distant metastases.

CT image acquisition

The non-CE images obtained before contrast material injection were used for texture analysis. Images had been localized at the level of the largest transverse dimension of the lung lesion (CT Twin: Elscint, Haifa, Israel) for 1 s duration (300 mA, 120 kVp, 10-mm section thickness). The in-plane resolution for the non-CE CT images used in this study was 0.84 mm.

FDG-PET acquisition and analysis

All patients had undergone a FDG-PET study after a fast of at least 6 h. Patients' weight and blood glucose level had been recorded; 150 to 250 MBq of FDG had been injected with imaging performed at 60 min after injection with a dedicated sodium iodide PET scanner (Quest; GE Medical Systems, Milwaukee, USA). Emission data had been collected for 4 min for each 12.5-cm field of view with 6.4-cm overlap. Transmission scanning had been performed either before or during acquisition of emission data using a caesium-137 rod source. Attenuation corrected images (128×128 pixels, slice thickness of 4 mm) had been produced by iterative reconstruction. The x–y resolution of the system using this reconstruction algorithm was approximately 6 mm full-width at half-maximum. The standardised uptake value (SUV) for FDG had been determined (after decay corrected activity concentration) for the largest transverse cross-section for each lung lesion similar to the location at which CT acquisition was performed. The SUV for a region of interest (ROI) constructed over this lung lesion was defined as follows:

$$SUV = \frac{\text{Activity concentration in the tissue [Bq/g]}}{\text{Administered activity [Bq]/body weight [g]}} \quad (1)$$

Only the mean SUV (SUV_{mean}) was available in this archived retrospective study rather than maximum SUV (SUV_{max}) that is more commonly used in current practice.

Lung lesion densitometry and texture analysis

For each lung lesion, x-ray attenuation and texture were assessed within the reconstructed 10-mm non-CE CT image transferred to a personal computer. Texture analysis comprised 2 stages: (a) image filtration using Laplacian of Gaussian (LoG) spatial band-pass filter, followed by (b) quantification of texture. This analysis methodology previously used for hepatic texture analysis[18], processed each conventional CT image to produce a series of derived filtered images displaying fine, medium and coarse texture features, respectively (Fig. 1). This algorithm was developed and implemented in-house initially as a research prototype written in MATLAB (technical computing language, Mathworks Inc, Natick, USA) and currently developed as a standalone clinical prototype.

Within the ROI drawn around the lung lesion on conventional CT imaging, a thresholding procedure was carried out to exclude air by removing from analysis any pixels with attenuation values below −50 Hounsfield units (HU). The ROIs were drawn in a semi-automated manner whereby the operator initially draws a ROI roughly enclosing the lesion while excluding the bones. In an automated approach the ROI updates itself based on the above threshold (−50 HU), segmenting out the exact lesion removing any residual air that may have been included within the initial ROI.

In brief, the texture in each derived filtered image as well as the conventional CT image (i.e. without filtration) was quantified by calculating the mean grey-level
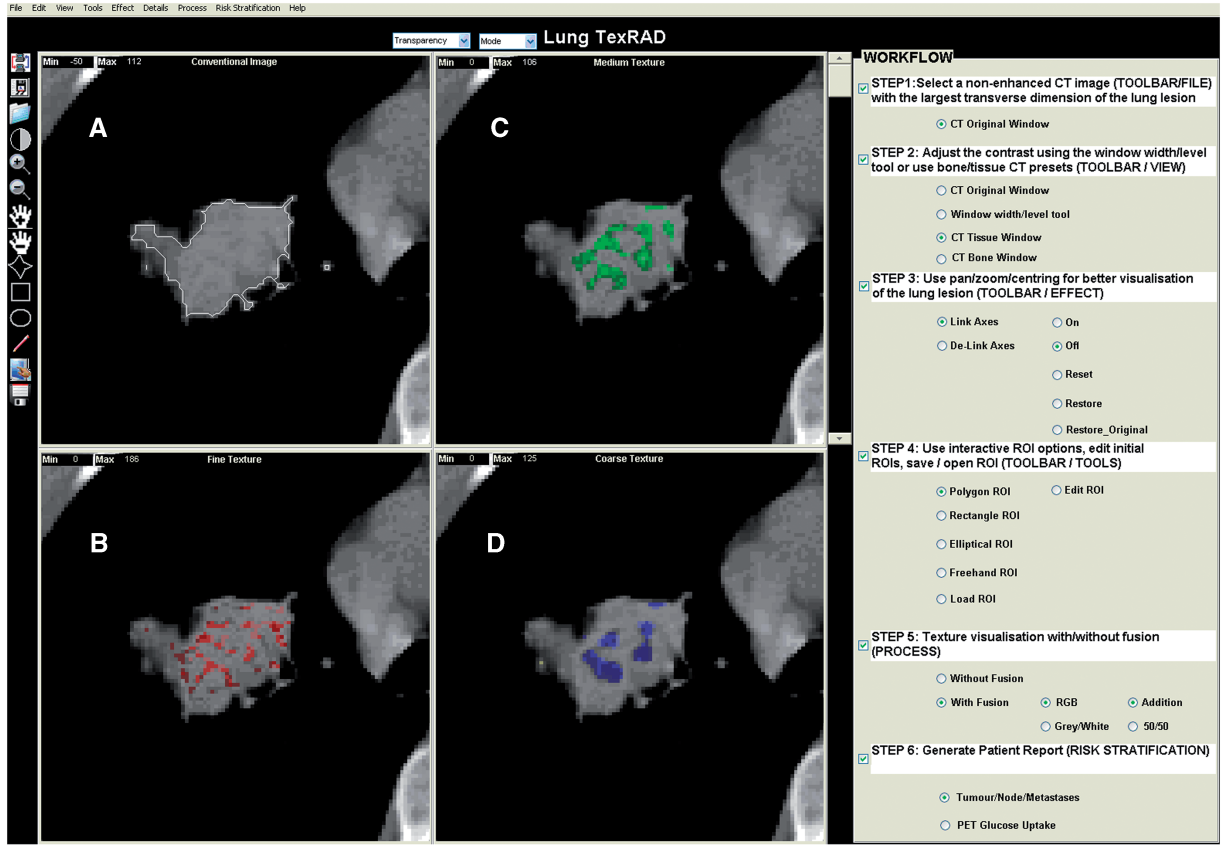
Figure 1 **(A) Conventional non-CE CT image with the lung lesion and corresponding images selectively displaying (B) fine, (C) medium and (D) coarse lung lesion texture, respectively. Fine, medium and coarse textures correspond to lung lesion features of different sizes and intensity variations extracted by the image filter thereby showing varying degrees of coarseness.**

intensity (MGI, i.e. brightness; without image filtration this parameter is the same as CT lung lesion density in HU also known as CT number), entropy (reflects intensity and inhomogeneity) and uniformity (reflects how close the image is to a uniform distribution of the grey levels) within the ROI. These parameters are defined below where R is the ROI within the image $a(x,y)$, N is the total number of pixels in R, l is the number of grey levels (e.g. $l = 1$ to k indicates grey level from 1 to k) in and $p(l)$ is the probability of the occurrence of the grey level l based on the image histogram technique:

$$\text{Mean grey} - \text{level intensity (MGI)} = \frac{1}{N} \sum_{(x,y)\in R} [a(x,y)] \quad (2)$$

$$\text{Entropy } (E) = -\sum_{l=1}^{k} [p(l)] \log_2 [p(l)] \quad (3)$$

$$\text{Uniformity } (U) = \sum_{l=1}^{k} [p(l)]^2 \quad (4)$$

Entropy and uniformity are additional statistical image parameters that give further insight into the distribution of tissue attenuation information lost when averaging

Table 1 *Image filter, corresponding size of the texture features extracted and parameters quantified*

Image filter (σ)	Size of features highlighted (pixels/mm)	Texture quantifiers
None	Not applicable	MGI, entropy, uniformity
Fine ($\sigma = 0.5$)	2/1.68	MGI, entropy, uniformity
Medium ($\sigma = 1.5$)	6/5.04	MGI, entropy, uniformity
Coarse ($\sigma = 2.5$)	12/10.08	MGI, entropy, uniformity

intensity over a large area. These features are perceived visually as image texture. A summary of all the texture parameters calculated is given in Table 1. A single operator under supervision from a researcher with 4 years experience in texture analysis of radiographic images performed the analyses. Both were blinded to the results of FDG-PET analysis.

Statistical analysis

Linear regression analysis was used to assess the statistical correlations between CT tumour texture and SUV on

FDG-PET. To rule out the possibility of an isolated association being obtained by chance when multiple independent tests are implemented, correlation trends between texture and SUV were observed. Bonferroni correction was not used because the texture parameters in this study were not completely independent, a prerequisite for its implementation. The relationship between texture and SUV with stage was assessed using the non-parametric Spearman's rank correlation test. Furthermore Kappa statistics along with an accuracy estimate provided the degree of agreement for the parameter (texture/SUV) demonstrating most significant association with staging in NSCLC. For the most significant predictor of tumour stage, sensitivity and specificity for the diagnostic threshold from the area under the receiver-operating characteristic (ROC) analysis were calculated along with the 95% confidence interval (CI). For all statistical tests, a p-value less than 0.05 was considered to be significant.

Results

Mean (range) tumour SUV for all the patients was 6.6 (2.8–10.4). Based on CT and FDG-PET imaging, the number of patients with tumour stages I, II, III and IV were 4, 4, 4 and 6 respectively.

Tumour attenuation and texture without filtration on CT did not show any significant association with SUV (Table 2). Medium to coarse textures demonstrated an increasing association with SUV for all texture quantifiers (MGI, entropy and uniformity; Table 2), however, reaching statistical significance only for coarse texture features (Fig. 2A: uniformity, $r = -0.521$, $p = 0.027$; entropy, $r = 0.512$, $p = 0.030$).

Of all tumour texture and densitometry analyses, only fine texture features correlated significantly with tumour stage (Table 3; Fig. 2B: MGI, $r_s = 0.71$, $p = 0.001$; entropy, $r_s = 0.5$, $p = 0.02$, uniformity, $r_s = -0.49$, $p = 0.04$). Furthermore SUV also correlated significantly with tumour stage ($r_s = 0.56$, $p = 0.02$).

Fine MGI demonstrated a substantial degree of concordance with PET tumour staging (stage I, MGI <3.2591; stage II, $3.2591 \leq MGI \leq 4.2632$; stage III, $4.2632 < MGI \leq 4.9345$; stage IV: MGI > 4.9345, kappa $= 0.7$, 95% CI $= 0.44–0.96$, accuracy $= 77.8\%$, 95% CI $= 54.8–91.0$). Furthermore a fine MGI above 4.2632 predicted tumours above stage II with an area under the ROC curve of 0.925 ($p = 0.0001$), sensitivity of 100% (95% CI $= 69–100$) and specificity of 87.5% (95% CI $= 47.4–97.9$).
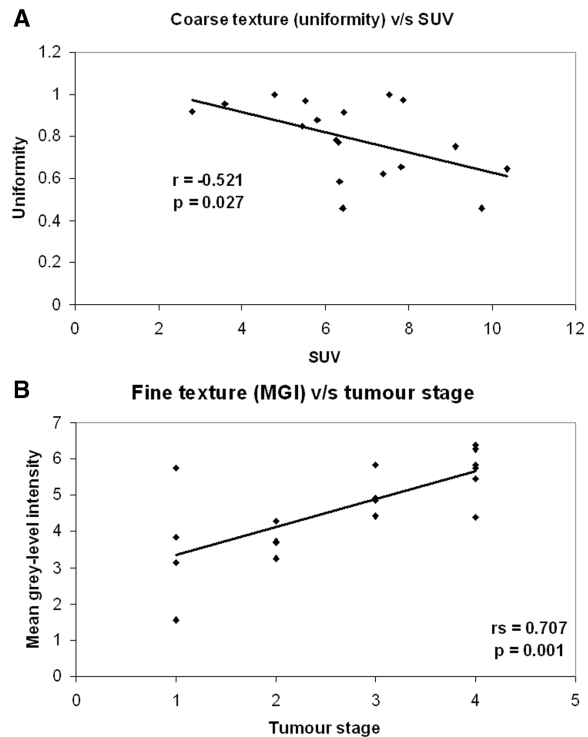

Figure 2 **Graph showing association between (A) coarse (uniformity) tumour texture and SUV and (B) fine (MGI) tumour texture and stage.**

Table 2   Linear regression (r) values and p values for lung tumour density and texture on CT computed as MGI, entropy and uniformity against glucose uptake (SUV) on FDG-PET for all patients

Tumour densitometry/ texture (filter width)		MGI	Entropy	Uniformity
Density and texture	r	0.234	−0.046	0.100
without filtration	p	0.350	0.856	0.694
Fine texture	r	0.141	0.310	−0.287
	p	0.577	0.211	0.248
Medium texture	r	0.131	0.285	−0.310
	p	0.603	0.252	0.211
Coarse texture	r	0.428	**0.512**	**−0.521**
	p	0.077	**0.030**	**0.027**

Bold values indicate a statistically significant correlation.

Table 3   Spearman rank order correlation coefficient (r_s) values and p values for lung tumour density and texture on CT computed as MGI, entropy and uniformity against PET tumour stage for all patients

Tumour Densitometry/ texture (filter width)		MGI	Entropy	Uniformity
Density and texture	r_s	−0.028	0.412	−0.408
without filtration	p	0.914	0.089	0.092
Fine texture	r_s	**0.707**	**0.549**	**−0.487**
	p	**0.001**	**0.018**	**0.04**
Medium texture	r_s	0.096	0.280	−0.306
	p	0.702	0.259	0.219
Coarse texture	r_s	0.408	0.391	−0.402
	p	0.092	0.108	0.098

Bold values indicate a statistically significant correlation.

Discussion

Computer analysis of the lungs on CT has been used for segmentation of pulmonary structures, image registration and disease detection, classification and quantification[19]. In the case of lung cancer, lesion classification has entailed estimation of the probability of malignancy for which purpose some authors have used texture analysis[20–22]. Our pilot study has demonstrated the potential for the application of texture analysis to be extended beyond simple distinctions of benign and malignant lesions to a more detailed characterisation of lung cancers with identification of adverse tumour characteristics such as increased glucose metabolism and advanced stage.

To address the more complex issues of developing imaging markers assessing lung tumour aggression, we used selective-scale based image filtration prior to texture quantification. Image filtration separately evaluated textures at different scales from fine to coarse. This is similar to a non-orthogonal Wavelet approach having the flexibility of fine-tuning the filter to extract visually imperceptible image features at particular scales that may correspond to specific tumour biology. This specific filtration proved to be necessary as indicated by the fact that no significant correlations were found between density/textural parameters without image filtration and tumour SUV/stage. By using image filtration, we were able to adopt first order statistical texture quantification. These parameters benefit from being directionally independent and have the advantage of being less computationally expensive. In addition this selective-scale texture quantification approach also benefits from lack of a priori nature of the mathematical model and shape description of local structure boundaries.

The finding of increased glucose metabolism in tumours with altered medium-coarse texture may relate to metabolic change associated with the areas of low CT attenuation in the presence of necrosis, haemorrhage and myxoid[13,15]. Areas of tumour necrosis in particular are known to be associated with increased glucose metabolism in adjacent tumour tissue[14,23]. The biological rationale for the association between mean fine texture intensity and tumour stage is not very apparent, but potentially may reflect multiple small areas of diffuse necrosis in higher clinical stage tumours. Nevertheless, these potential associations between texture and pathology need to be confirmed in further studies.

The use of imaging in cancer risk stratification is currently limited to TNM staging. The widespread use of cardiac CT for calcium scoring for obtaining information about the presence, location, extent of calcified plaque in coronary artery disease suggests the potential increase in the utility of imaging as a risk stratification tool. When previously applied to CT images of the liver, the texture analysis methodology used in our study has been shown to correlate with liver physiology, specifically a combination of blood flow and glucose metabolism that reflects hepatic glucose phosphorylation, and to be a potential marker of survival and provide risk stratification information for patients following resection of colorectal cancer[24,25].

The correlation between texture and FDG uptake in this study suggest a potential for texture analysis to provide prognostic information analogous to that provided by FDG-PET for which a high SUV has been shown to indicate an adverse outcome for patients with NSCLC[16]. Similarly, texture analysis could potentially be used to predict response of NSCLC to therapy as has recently been shown for FDG uptake and response to gefitinib[17]. The texture parameter correlating most closely with SUV was coarse texture quantified as uniformity. A previous phantom study has shown that this parameter has low variability with change in CT acquisition parameters, providing further support for the clinical applicability of texture analysis[24]. Further research will be needed to confirm an association between texture and survival in a larger series of patients and to determine whether any prognostic or risk stratification information from texture analysis of CT images would be complementary to, or supersede that obtained from FDG-PET measurements of SUV.

Although the patients in this preliminary study had undergone both CT and FDG-PET, our results suggest a potential for texture analysis to improve the accuracy of CT staging for patients with NSCLC undergoing assessment by CT alone. Currently, nodal staging based on size criteria alone has low accuracy because nodes with a maximum transverse diameter of less than 10 mm may contain metastatic tumour; nodes greater than 10 mm can be reactive. For this reason, FDG-PET is increasingly recommended for staging patients with NSCLC. Our study suggests a high concordance between texture and tumour stage as assessed by FDG-PET (kappa 0.7) with high accuracy for identifying patients with tumours above stage II in particular, for whom surgery is unlikely to be of benefit. Criteria that combine nodal size with texture measurements in the primary tumour could potentially improve this staging accuracy further. Although CT with texture analysis is unlikely to replace FDG-PET, conventional CT is frequently used to select patients for PET imaging. The incorporation of texture analysis into these CT examinations has the potential to improve this selection process.

One limitation to our study has been the use of FDG-PET rather than histological analysis of surgical specimens to ascertain tumour stage. However, surgical staging is only feasible for patients with early stage tumours because those with more advanced tumours are not considered surgical candidates. PET is considered the most accurate staging technique that can be applied to all patients with NSCLC[26]. It would also be useful to ascertain if the use of CE CT improves the prognostic power of our technique and whether the results of our study

apply to other types of lung tumour such as small cell lung cancer. The texture analysis methodology extracts CT lung lesion features based on size (minimum 2 pixels or 1.68 mm and maximum 12 pixels or 10.08 mm in width) and intensity variation. For a statistically sensible analysis and to extract texture features comparable with fine–coarse sizes, the ROI needs to be large enough. This could potentially be a limitation for analysis of lung nodules, where the entire range of the filter sizes used in this study may not be applicable. A further limitation is the use of a single two-dimensional CT image of the lung tumour rather than three-dimensional analysis of a CT volume. We have implemented our texture analysis methodology for lung CT in 3 dimensions with application to other pulmonary pathologies and future work will comprise extending the application of three-dimensional analysis to lung cancer[27].

Conclusions

This study provides initial evidence for a relationship between texture features in NSCLC on non-CE CT and tumour metabolism and stage. Texture analysis warrants further investigation as a potential method for obtaining prognostic information for patients with NSCLC undergoing CT.

References

[1] Matteis SD, Consonni D, Bertazzi PA. Exposure to occupational carcinogens and lung cancer risk. Evolution of epidemiological estimates of attributable fraction. Acta Biomed 2008; 79: 34–42.

[2] WHO. Revised global burden of disease (GBD) 2002 estimates. 2008. Available from: http://www.who.int/healthinfo/bodgbd 2002revised/en/index.html.

[3] Travis WD, Travis LB, Devesa SS. Lung cancer. Cancer 1995; 75: 191–202. doi:10.1002/1097-0142(19950101)75:1+<191::AID-CNCR2820751307>3.0.CO;2-Y.

[4] Giger ML, Bae KT, MacMahon H. Computerized detection of pulmonary nodules in computed tomography images. Invest Radiol 1994; 29: 459–65. doi:10.1097/00004424-199404000-00013. PMid:8034453.

[5] Armato III SG, Giger ML, MacMahon H. Automated detection of lung nodules in CT scans: preliminary results. Med Phys 2001; 28: 1552–61. doi:10.1118/1.1387272. PMid:11548926.

[6] Lou S-L, Chang C-L, Lin K-P, Chen T-S. Object-based deformation technique for 3-D CT lung nodule detection. SPIE Proc 1999; 3661: 1544–52. doi:10.1117/12.348557.

[7] Brown MS, McNitt-Gray MF, Goldin JG, et al. Patient-specific models for lung nodule detection and surveillance in CT images. IEEE Trans Med Imaging 2001; 20: 1242–50. doi:10.1109/42.974919. PMid:11811824.

[8] Cavouras D, Prassopoulos P, Pantelidis N. Image analysis methods for solitary pulmonary nodule characterization by computed tomography. Eur J Radiol 1992; 14: 169–72. doi:10.1016/0720-048X(92)90079-O.

[9] Henschke CI, Yankelevitz DF, Mateescu I, et al. Neural networks for the analysis of small pulmonary nodules. Clin Imaging 1997; 21: 390–9. doi:10.1016/S0899-7071(97)81731-7.

[10] McNitt-Gray MF, Hart EM, Wyckoff N, et al. A pattern classification approach to characterizing solitary pulmonary nodules imaged on high resolution CT: preliminary results. Med Phys 1999; 26: 880–8. doi:10.1118/1.598603. PMid:10436888.

[11] Armato III SG, Li F, Giger ML, et al. Lung cancer: performance of automated lung nodule detection applied to cancers missed in a CT screening program. Radiology 2002; 225: 685–92. doi:10.1148/radiol.2253011376. PMid:12461246.

[12] Armato III SG, Altman MB, LaRiviere PJ. Automated detection of lung nodules in CT scans: effect of image reconstruction algorithm. Med Phys 2003; 30: 461–72. doi:10.1118/1.1544679. PMid:12674248.

[13] Kim HC, Lee JM, Kim SH, et al. Small gastrointestinal stromal tumours with focal areas of low attenuation on CT: pathological correlation. Clin Radiol 2005; 60: 384–8. doi:10.1016/j.crad.2004.06.022. PMid:15710143.

[14] Zhao S, Kuge Y, Mochizuki T, et al. Biologic correlates of intratumoural heterogeneity in ^{18}F-FDG distribution with regional expression of glucose transporters and hexokinase-II in experimental tumour. J Nucl Med 2005; 46: 675–82.

[15] Kim TH, Kim SJ, Ryu YH, et al. Pleomorphic carcinoma of lung: comparison of CT features and pathologic findings. Radiology 2004; 232: 554–9. doi:10.1148/radiol.2322031201. PMid: 15215543.

[16] Berghmans T, Dusart M, Paesmans M, et al. Primary tumour standardized uptake value (SUVmax) measured on fluorodeoxyglucose positron emission tomography (FDG-PET) is of prognostic value for survival in non-small cell lung cancer (NSCLC): a systematic review and meta-analysis (MA) by the European Lung Cancer Working Party for the IASLC Lung Cancer Staging Project. J Thorac Oncol 2008; 3: 6–12. doi:10.1097/JTO.0b013e31815e6d6b. PMid:18166834.

[17] Na II, Byun BH, Kang HJ, et al. ^{18}F-Fluoro-2-deoxy-glucose uptake predicts clinical outcome in patients with gefitinib-treated non-small cell lung cancer. Clin Cancer Res 2008; 14: 2036–41. doi:10.1158/1078-0432.CCR-07-4074. PMid:18381942.

[18] Ganeshan B, Miles KA, Young RCD, Chatwin CR. Texture analysis in non-contrast enhanced CT: Impact of malignancy on texture in apparently disease-free areas of the liver. Eur J Radiol 2009; 70: 101–10. doi:10.1016/j.ejrad.2007.12.005. PMid: 18242909.

[19] Sluimer I, Schilham A, Prokop M, van Ginneken B. Computer analysis of computed tomography scans of the lung: a survey. IEEE Trans Med Imaging 2006; 25: 385–405. doi:10.1109/TMI.2005.862753. PMid:16608056.

[20] McNitt-Gray MF, Wyckoff N, Sayre JW, Goldin JG, Aberle DR. The effects of co-occurrence matrix based texture parameters on the classification of solitary pulmonary nodules imaged on computed tomography. Comput Med Imaging Graph 1999; 23: 339–48. doi:10.1016/S0895-6111(99)00033-6.

[21] Kido S, Kuriyama K, Higashiyama M, Kasugai T, Kuroda C. Fractal analysis of small peripheral pulmonary nodules in thin-section CT: evaluation of the lung-nodule interfaces. J Comput Assist Tomogr 2002; 26: 573–8. doi:10.1097/00004728-200207000-00017. PMid:12218822.

[22] Wang H, Guo XH, Jia ZW, et al. Multilevel binomial logistic prediction model for malignant pulmonary nodules based on texture features of CT image. Eur J Radiol 2010; 74: 124–9. doi:10.1016/j.ejrad.2009.01.024. PMid:19261415.

[23] Galiè M, Farace P, Nanni C, et al. Epithelial and mesenchymal tumour compartments exhibit in vivo complementary patterns of vascular perfusion and glucose metabolism. Neoplasia 2007; 9: 900–8.

[24] Miles KA, Ganeshan B, Griffiths MR, Young RCD, Chatwin CR. Colorectal cancer: texture analysis of portal phase hepatic CT images as a potential marker of survival. Radiology 2009; 250: 444–52. doi:10.1148/radiol.2502071879. PMid:19164695.

[25] Ganeshan B, Miles KA, Young RCD, Chatwin CR. In search of biological correlates for liver texture on portal-phase CT. Acad Radiol 2007; 14: 1058–68. doi:10.1016/j.acra.2007.05.023. PMid:17707313.

[26] Gould MK, Kuschner WG, Rydzak CE, *et al.* Test performance of positron emission tomography and computed tomography for mediastinal staging in patients with non-small-cell lung cancer: a meta-analysis. Ann Intern Med 2003; 139: 879–92.

[27] Ganeshan B, Miles KA, Young RC, Chatwin CR. Three-dimensional selective-scale texture analysis of computed tomography pulmonary angiograms. Invest Radiol 2008; 43: 382–94. doi:10.1097/RLI.0b013e3181690091. PMid:18496043.